Mechanism of LolCDE as a molecular extruder of bacterial triacylated lipoproteins

Stuti Sharma[1,*], Ruoyu Zhou[2,*], Li Wan[2], KangKang Song[3,4], Chen Xu[3,4], Yanyan Li[2,#] & Maofu Liao[1,#]

[1]Department of Cell Biology, Blavatnik Institute, Harvard Medical School, Boston MA, USA
[2]Key Laboratory of Structural Biology of Zhejiang Province, School of Life Sciences, Westlake University, Hangzhou 310024, China
[3]Department of Biochemistry and Molecular Pharmacology, University of Massachusetts Medical School, Worcester MA, USA
[4]Cryo-EM Core Facility, University of Massachusetts Medical School, Worcester MA, USA

*These authors contributed equally to this work
[#]Correspondence to: liyanyan@westlake.edu.cn; maofu_liao@hms.harvard.edu

Abstract

Present in all bacteria, lipoproteins are central in bacterial growth and antibiotic resistance. These proteins use lipid acyl chains attached to the N-terminal cysteine residue to anchor on the outer surface of cytoplasmic membrane. In Gram-negative bacteria, many lipoproteins are transported to the outer membrane (OM), a process dependent on the ATP-binding cassette (ABC) transporter LolCDE which extracts the OM-targeted lipoproteins from the cytoplasmic membrane for subsequent trafficking across the periplasm. Lipid-anchored proteins pose a unique challenge for transport machinery as they have both hydrophobic lipid moieties and soluble protein component, and the underlying mechanism is poorly understood. Here we determined the cryo-EM structures of nanodisc-embedded LolCDE in the nucleotide-free and nucleotide-bound states at 3.8-Å and 3.5-Å resolution, respectively. The structural analyses, together with biochemical and mutagenesis studies, uncover how LolCDE specifically recognizes its substrate by establishing multiple interactions with the lipid and N-terminal peptide moieties of the lipoprotein, and identify the amide-linked acyl chain as the key element for LolCDE interaction. Upon nucleotide binding, the transmembrane helices and the periplasmic domains of LolCDE undergo large-scale, asymmetric movements, resulting in extrusion of the captured lipoprotein. Comparison of LolCDE and MacB reveals the conserved mechanism of type VII ABC transporters and emphasizes the unique properties of LolCDE as a molecule extruder of triacylated lipoproteins.

Introduction

Found in all bacteria, lipoproteins are anchored in the cytoplasmic membranes using the lipid moiety attached to the N-terminal cysteine residue. Lipoproteins are a significant proportion (1% - 3%) of bacterial proteomes[1] and play central roles in bacterial physiology, including cell envelope formation, lipopolysaccharide biogenesis, nutrition acquisition, biofilm formation, stress response, and modulation of immune response of the host[2, 3]. After being generated in the cytosol, lipoproteins are translocated across the membrane through SecYEG or twin-arginine systems, and subsequently acylated by sequential actions of a series of modification enzymes[4, 5] (Fig. 1a). These enzymatic reactions result in tri-acylation of the N-terminal invariant cysteine residue in the lipoproteins, with two acyl chains ester-linked to the cysteine side chain and one acyl chain amide-linked to the N-terminus of lipoprotein. However, variable enzymes in different bacteria can lead to variation in the number and position of lipoprotein acylation[6, 7].

In Gram-negative bacteria, many lipoproteins are transported to the outer membrane (OM), being positioned in the periplasmic leaflet to face the periplasm or in the outer leaflet to become surface exposed[8]. Lipoprotein transport from the inner membrane (IM) to the OM depends on a set of proteins in the Lol (localization of lipoprotein) pathway and is best studied in *E. coli*[9] (Fig. 1a). The OM-targeted lipoproteins are first extracted out of the IM, a process driven by the ATP-binding cassette (ABC) transporter complex LolCDE. All ABC transporters contain two transmembrane domains (TMDs) and two nucleotide binding domains (NBDs). The transmembrane helices (TMs) of LolC and LolE form the TMDs, and two LolD proteins function as the NBDs. In addition, LolC and LolE each have a large periplasmic domain. The periplasmic chaperone LolA binds to the periplasmic domain of LolC, picks up extracted lipoprotein, and delivers it to the OM acceptor LolB which itself is a lipoprotein. Finally, the lipoprotein is inserted into the OM. While *E. coli* can grow without LolA and LolB under certain conditions, LolCDE is strictly essential for bacterial survival[10]. Due to its importance in OM localization of lipoproteins and antibiotic resistance, LolCDE is an attractive target for developing novel class of antibacterial drugs[11-13].

To fulfill its physiological function, LolCDE must not only specifically recognize mature lipoproteins, but also distinguish the lipoproteins that are destined to the OM from those which remain in the IM. The mechanism underlying these two fundamental aspects of LolCDE is poorly understood. In *E. coli*, the final acylation enzyme Lnt, which adds the third acyl chain to the N-terminal amine group, is an essential protein for bacterial growth, unless LolCDE is overexpressed[14]. Thus, N-acylation of lipoprotein likely serves as a checkpoint to ensure that LolCDE interacts with only mature lipoproteins. For the determinants of specific interaction between LolCDE and OM lipoproteins, our knowledge is limited. In *E. coli*, the presence of an aspartate residue in the second amino acid position (i.e., +2 position) immediately after the invariant cysteine residue, causes lipoprotein retention in the IM[9]. However, this well-known "+2 rule" is applicable to only *E. coli* and related enterobacteria. For other species, analyses based on primary amino acid sequence of the N-terminal lipoprotein residues fails to generate definitive patterns to predict the outcome of lipoprotein transport[15-18], suggesting that lipoprotein sequence alone is not sufficient for determining lipoprotein interaction with the transporter.

While numerous transporters that mediate cross-membrane movement of lipids or proteins have been extensively studied, lipoproteins containing both lipid and protein moieties represent a special group of substrates for membrane transport, and the underlying mechanism remains an enigma. The topological organization of LolCDE is distinct from that of most ABC transporters, and LolCDE is predicted to have similar folding as MacB, a homodimeric ABC transporter in a tripartite multidrug transporter complex in Gram-negative bacteria[19]. Based on TMD architecture, MacB is assigned as the only type VII ABC transporter with known strucutres[20, 21]. Mainly due to the lack of a substrate bound MacB structure, the mechanisms underlying substrate recognition and transport of this type of ABC transporters remain obscure. Importantly, unlike MacB which accepts a variety of compounds

from the periplasm, LolCDE specifically extracts lipoproteins from the IM, and thus the functional mechanisms for these two ABC transporters must be divergent.

In this work, we determined the cryo-EM structures of nucleotide-free and ADP-vanadate-bound *E. coli* LolCDE in a native-like lipid bilayer, at 3.8-Å and 3.5-Å resolutions, respectively. Structural analyses reveal the architecture of LolCDE, high-resolution details of lipoprotein-transporter interaction at the interface between LolC and LolE, and large-scale conformational transition induced by nucleotide binding. Together with biochemical assays and mutagenesis studies, our results reveal the fundamental mechanism of LolCDE by which the lipoprotein substrate is specifically captured and extracted from the membrane. Furthermore, the comparison between LolCDE and MacB provides important insights of how type VII ABC transporters function.

Purification and structural determination of LolCDE in nanodiscs

E. coli LolCDE complex was overexpressed in *E. coli* strain BL21(DE3), purified in dodecyl maltoside (DDM) detergent, reconstituted into nanodiscs with palmitoyl-oleoyl-phosphatidylglycerol (POPG), and screened in negative stain for monodisperse particles of similar size and shape (Supplementary Fig. 1a, b). The analysis of the kinetics of ATP hydrolysis by LolCDE in nanodiscs yielded a *Km* value of 0.19 +/- 0.05 mM and a *Vmax* value of 242.8 +/- 15.3 mole phosphate per min per mole protein (Fig. 1c). This activity is ~2.7 times the activity of LolCDE in DDM (Fig. 1b), suggesting that membrane environment is important to maintain the native conformation and full activity of the transporter. LolCDE was sensitive to the inhibition by vanadate, and 0.1 mM orthovanadate led to ~90% suppression of the activity of LolCDE (Fig. 1b and Supplementary Fig. 1c). The nanodisc-embedded LolCDE was subjected to single-particle cryo-EM analysis, generating a cryo-EM three-dimensional (3D) reconstruction at an overall resolution of 3.8 Å (Fig. 1d and Supplementary Fig. 2). The TMs of LolC and LolE are with higher resolution and have well-defined side-chain densities for most amino acid residues, enabling *de novo* model building and unambiguous registry of amino acids (Supplementary Fig. 2g). LolD and the periplasmic domains of LolC and LolE are with lower resolution, likely due to higher mobility, and their models were built based on published domain structure and homology model as detailed in Methods.

Overall structure of LolCDE

The structure of *E. coli* LolCDE displays pseudo-two-fold symmetry (Fig. 1d), and the homologous LolC and LolE each interact with one LolD protein in the cytosol, using coupling helix between TM2 and TM3 and C-terminal sequence (Fig. 1g). As shown in the domain arrangement (Fig. 1e), LolC and LolE each contain an N-terminal elbow helix, four TMs (TM1-4), a large periplasmic domain between TM1 and TM2, and a shoulder sequence between TM3 and TM4. In the center of LolCDE are TM1 and TM2, against which TM3 and TM4 are packed (Fig. 1f). The overall structure and TMD topology of LolCDE are similar to those of MacB, the founding member of type VII ABC transporters[19, 20] (Supplementary Fig. 3).

While the structures of LolC and LolE, particularly in their TMDs, are highly homologous, with a root-mean-square-deviation (RMSD) of 1.12 Å over 145 Cα atoms of all TMs (Supplementary Fig. 3a-c), notable differences lie in their periplasmic domains and shoulder sequences. The periplasmic domains of LolC and LolE are oriented differently (Supplementary Fig. 3d). The β-hairpin loop in LolC (termed the "Hook"), which binds to LolA for lipoprotein transport[22], is positioned sideway, while the Hook counterpart in LolE, not involved in LolA binding, is pointed upward (Fig. 1d). The shoulder sequence between the TM3 and TM4 of LolC has 18 amino acid residues (342-360) forming a loop structure. In comparison, the shoulder sequence of LolE is much longer and contains two parts: a 12-residue shoulder helix (344-356), which is located at the membrane surface, and a highly

ordered 21-residue shoulder loop (357-378), which rises above the membrane surface by ~16 Å. As detailed below, the shoulder sequences play a crucial role in lipoprotein interaction.

Three acyl chains of lipoprotein accommodated in two hydrophobic pockets

A density of co-purified lipoprotein was clearly resolved in our cryo-EM structure of LolCDE, showing all three acyl chains sandwiched between LolC and LolE (Fig. 1d, f, and Fig. 2a). Notably, the three acyl chains attached to the invariant cysteine residue are lifted to the level of membrane surface, adopting a nearly horizontal orientation (Fig. 2c, h). Thus, our structure captured an intermediate transport state of LolCDE, in which the lipoprotein substrate has been elevated to the interface between the IM and the periplasm but not yet released from the TMDs of the transporter.

The N-terminal cysteine residue and its three acyl chains are the conserved features of all mature *E. coli* lipoproteins, and thus expected to contribute to specific recognition of lipoproteins by LolCDE. This is consistent with the observation that the N-terminal peptide of lipoprotein and the acyl chains form intimate interactions with LolCDE and are well resolved in the cryo-EM map. The three acyl chains are separated into two groups and accommodated in two hydrophobic pockets (Fig. 3a, b). One of the two cysteine side chain-connected acyl chains (termed "R1") is located in the "front pocket" formed by the TM1 and shoulder loop of LolC and the TM2 of LolE (Fig. 2a, d, e and Supplementary Fig. 4f). The other side chain-connected acyl chain (termed "R2") and the N-terminal amine group-linked acyl chain (termed "R3") are packed together in the "back pocket" formed by the TM1 and shoulder loop of LolE and the TM2 of LolC (Fig. 2b, f, g and Supplementary Fig. 4g). Due to longer shoulder sequence in LolE and greater distance between the TMs, the back pocket accommodates a much larger volume than the front one. In the front pocket, R1 forms close contact with several hydrophobic residues from LolC (Val44, Val47, Met48 and Phe51 in TM1 and Leu351 in shoulder loop) and from LolE (M267 and Ile271 in TM2) (Fig. 2d, e). In the back pocket, the interactions are predominantly mediated between R3 and the shoulder loop of LolE, involving Phe360, Leu361, Ile365, Tyr366, Phe367 and Leu 371 (Fig. 2g). In comparison, R2 makes much less contact. Additional hydrophobic interactions with R3 and R2 are contributed by the TM2 of LolC (Met262, Met266 and Leu270) and the TM1 of LolE (Val43, Met48 and Phe51) (Fig. 2f). Most of the hydrophobic residues that form the substrate-binding pocket are highly conserved (Supplementary Fig. 5). Using single-site mutagenesis, the hydrophobic residues in close contact with the acyl chains of lipoprotein were changed to asparagine residue and tested for their stable interaction with the OM lipoprotein Lpp by co-purification (Fig. 2j, k). On either side of R1, F51N of LolC suppressed Lpp binding (Fig. 2j), but M267N of LolE had no effect (Fig. 2k). Interestingly, all single mutations in the shoulder loop of LolE (F360N, L361N, Y366N and L371N) abolished Lpp binding (Fig. 2k), and, also in the back pocket, M266N of LolC showed moderate decrease in Lpp interaction (Fig. 2j). These results indicate the critical importance of the LolE shoulder loop and back pocket in lipoprotein interaction.

Our structure reveals that three acyl chains of lipoproteins occupy two hydrophobic pockets in LolCDE with the last attached acyl chain (R3) making the most extensive interactions. These observations explain the preference of LolCDE for mature, triacylated lipoprotein, as well as the differential functional requirement of individual acyl chains in lipoprotein for transport. In *E. coli*, deletion of Lnt, and thus removal of R3 from lipoproteins (Fig. 1a), is lethal, and can be rescued by overexpression of LolCDE[14]. Interestingly, the lack of Lnt can also be complemented by expressing a transacylase, Lit, which transfers one of the two side chain-linked acyl chains to the amine group (R3)[23]. These findings corroborate the notion that, among the three acyl chains in lipoprotein, R3 in the back pocket forms the strongest interaction with LolCDE and is crucial for lipoprotein transport.

Interaction of N-terminal peptide of lipoprotein with LolCDE

In our cryo-EM map of LolCDE, a strong density is resolved following the triacylated cysteine residue, corresponding to 6 N-terminal amino acid residues of lipoprotein. This density is not with sufficient resolution for accurate amino acid assignment, likely due to different lipoproteins bound to the purified LolCDE. Lpp is the most abundant lipoprotein in *E. coli*[24, 25], and can form stable complex in our co-purification assay (Fig. 2j, k). Because Lpp contains a serine residue in the +2 position, we modeled the first 6 residues of the lipoprotein as Cys-Ser-Ala-Ala-Ala-Ala.

The first four residues (+1 to +4 positions) are at approximately the same height above the membrane surface. They adopt a kinked conformation to tightly fit into a relatively shallow hydrophobic pocket (Fig. 3b, best shown in the fourth panel), which is formed by the TM1 and TM2 of LolC and the shoulder loop and TM2 of LolE (Fig. 2i and Supplementary Fig. 4h). While the +1 cysteine residue is in closer proximity to the TM2 of LolE, the +2 residue is rotated away and positioned near Ile365 and Tyr366 (shoulder loop) of LolE. The following N-terminal peptide takes a right-handed turn such that the +3 and +4 residues come in close contact with Val260 (TM2) and Phe51 (TM1) of LolC, respectively. The following ~10 residues extend upward and reach the periplasmic domain of LolE, where it makes contact with a patch of hydrophobic residues consisting of Ile247, Tyr248, Val249 and Tyr250 (Supplementary Fig. 4d). The further C-terminal region of lipoprotein is not resolved, suggesting that the main body of lipoproteins is located outside the periplasmic domains and does not interact with LolCDE. These are consistent with the notion that LolCDE recognizes highly variable lipoproteins through specific interactions with only their N-terminal peptide and lipid moieties. Furthermore, localization of N-terminal region of lipoprotein on the front side of LolCDE, together with the large shoulder sequence of LolE shielding the back side, seems to suggest that lipoproteins enter the transporter from the front side through the interface between the TM1 of LolC and the TM2 of LolE.

Above the acyl chain binding pockets, the surface property at the interface of LolC and LolE transitions sharply from hydrophobic to hydrophilic with predominantly negative charge (Fig. 3c, d). The N-terminal cysteine residue is sandwiched between Glu263 in LolC and Asp264 in LolE (Supplementary Fig. 4b, c). Changing these two residues individually to alanine or lysine residue completely blocked Lpp co-purification (Fig. 2j), demonstrating the importance of negative charge for lipoprotein interaction. Additional negatively charged residues include Asp352 (shoulder loop of LolC), Glu54 (LolE-TM1) and Asp364 (shoulder loop of LolE) (Fig. 3d). While the mechanism by which the negatively charged surface supports lipoprotein binding is not clear, charge repulsion with the phosphate groups of the phospholipids in the IM may limit their entry to LolCDE and help select for lipoproteins with an uncharged cysteine residue at the +1 position.

LolCDE extrudes lipoprotein via drastic conformational transition

To understand how LolCDE extracts the bound lipoprotein out of the TMDs, we determined the cryo-EM structure of vanadate-trapped *E. coli* LolCDE at 3.5-Å resolution (Fig. 4a and Supplementary Fig. 6). The cryo-EM sample contained 1 mM vanadate, a concentration sufficient for ~90% inhibition of LolCDE (Supplementary Fig. 1c). Such inhibition is caused by ADP-vanadate complex trapped in ATP site and stabilizing an intermediate conformation of ATPase.

In the vanadate-trapped LolCDE structure, the two LolD proteins move towards each other and associate together, with one ADP-vanadate complex in each of the two ATP sites at the dimer interface (Supplementary Fig. 7d). LolD engages three regions of both LolC and LolE: coupling helix, C-terminal sequence, and elbow helix. Among these three structural elements, coupling helices display the most pronounced conformational shift, which in turn causes an upward and inward movement of TM2 helices (Fig. 4b, d and Supplementary Video 1). The

conformational changes in TM2 and coupling helix of LolC and LolE are asymmetric, with more movements observed in LolE than LolC. Specifically, the coupling helix in LolC pushes TM2 up by ~4 Å, and such movement in LolE leads to a remarkable upward shift of TM2 by ~6 Å, which is more than one helical turn (Fig. 4d). In addition to vertical movement, the TM2 helices of LolC and LolE also shift inward at the membrane-periplasm interface by ~6.3 Å and ~8 Å, respectively (Fig. 4b, d). In sharp contrast to the substantial conformational transition of TM2, all other TMs demonstrate little movement, with the exception of the TM1 of LolE, which displays an inward shift by ~6 Å following the TM2 of LolE but no upward movement (Fig. 4b). In nucleotide-free LolCDE, the lipoprotein bound between the two TM2 helices is already elevated to the level of membrane surface (Fig. 2c). Upon nucleotide binding, the upward shift of TM2 would push the lipoprotein out of the TMDs and into the space between the periplasmic domains. Therefore, the power stroke is initiated when two NBDs (i.e., LolD) dimerize upon ATP binding, and, via the TM2 helices across the membrane, the movement of NBDs in the cytosol is coupled to the extrusion of the bound lipoprotein in the periplasm.

The inward movement of TM2 helices results in a two-helix bundle in the center of the transporter, thereby collapsing all three pockets which, in the nucleotide-free conformation, accommodate three acyl chains and the N-terminal peptide of the bound lipoprotein. Accordingly, we do not observe lipoprotein in the structure of vanadate-trapped LolCDE. When the catalytically important Glu171 in LolD was mutated to glutamine residue (E171Q), LolCDE lost stable Lpp binding (Fig. 2k). This is consistent with the notion that the mutant LolCDE in the IM is stabilized in the ATP-bound conformation which cannot bind lipoprotein. Notably, TM2 closes the lateral opening between LolC and LolE in the outer membrane leaflet and blocks access of both shoulder loops to the substrate (Supplementary Fig. 7c, e), and the resulting destabilization of the shoulder loops is clearly manifested by the weaker cryo-EM density in the vanadate-trapped conformation (Supplementary Fig. 7f). Complete elimination of all lipoprotein accommodating pockets and closure of substrate entry gate may be important to prevent lipoprotein backloading and ensure transport completion before accepting a new substrate. Taken together, our cryo-EM structure of vanadate-trapped LolCDE represents a functional state after the extrusion of lipoprotein.

Large-scale movements of LolCDE in the periplasmic space

The drastic shifts of TM2 propagate into the periplasmic regions of LolCDE. In the position of Tyr260 at the periplasmic end of TM2 of LolE, ~10 Å above the membrane surface, a local structural rearrangement creates a 90° kink, which travels 10.5-Å distance upward and to the center (Fig. 4c). A corresponding 90° kink in LolC is present in the nucleotide-free conformation, and, upon vanadate trapping, also moves upward and inward to join the 90° kink from LolE. These two kinks together form a T-shaped structure, closing the membrane-proximal space and shrinking the opening on the front side of the inter-periplasmic domain space (Supplementary Fig. 7c).

The upward and inward movements of TM2 cause remarkable translocation and rotation of periplasmic domains, resulting in an overall closure of these two domains. The asymmetrical transitions of the two TM2 helices are also reflected in distinct movements of the two periplasmic domains. While the motion of LolC periplasmic domain is predominantly a translation toward the center by ~12 Å with a small rotation of ~6° (Fig. 4e), the periplasmic domain of LolE moves mainly by a rotation of ~29.5° (Fig. 4f and Supplementary Video 1). The motion in LolC relocates the LolA-binding Hook near the top of the transporter (Fig. 4e). The crystal structure of LolA in complex with the periplasmic domain of LolC[22] can be docked on our nucleotide-free and vanadate-trapped LolCDE structures without obvious clashes (Supplementary Fig. 8), which is consistent with the previous findings that LolA-LolCDE interaction is not affected by the nucleotide binding to LolCDE[22]. Thus, the release of LolA-lipoprotein complex from LolC is likely caused by the conformational change of LolA upon lipoprotein loading, rather than the periplasmic domain movements alone. In addition, the lipoprotein linker-binding loop in the

periplasmic domain of LolE moves diagonally upward by ~8 Å, likely facilitating lipoprotein extraction by directly pulling the N-terminal peptide (Supplementary Fig. 4e). Together, the structural rearrangements of LolC and LolE in the periplasmic space seem to help lipoprotein extrusion, protect the acyl chains of extracted lipoprotein from the aqueous environment of the periplasm, and reorient the lipoprotein for interaction with the LolC-bound LolA.

Discussion

Bacterial lipoproteins represent a special group of macromolecules for cross-membrane translocation, due to their amphipathic nature. Our results provide insights of how lipoproteins are specifically transported by a dedicated molecular machine. We propose a model of lipoprotein extraction by *E. coli* LolCDE (Fig. 5) in which (1) lipoprotein in the periplasmic leaflet of the IM laterally enters the transporter through the interface between LolC and LolE on the front side; (2) the acyl chains of lipoproteins form extensive hydrophobic interactions with the front and back pockets in the transporter, resulting in elevation of the lipoprotein to the level of membrane surface; (3) ATP binding-induced LolD dimerization causes TM2 to move upward, which in turn pushes the bound lipoprotein out of the TMDs and into the space between the two rearranged periplasmic domains. Finally, ATP hydrolysis leads to dissociation of NBD dimer, resetting the conformation of LolCDE for the next cycle of transport.

Our results reveal how LolCDE recognizes highly variable OM-targeted lipoproteins through three distinct pockets that interact with the conserved structural features in lipoproteins: acyl chains and the N-terminal peptide. Importantly, we identified the N-terminal amine group-linked acyl chain (R3) as the predominant element to mediate hydrophobic interaction with the transporter, which explains why LolCDE prefers fully mature lipoproteins after the final acylation step. The first four residues of lipoprotein form a kink to fit tightly in a hydrophobic pocket with a front opening, suggesting that the N-terminal peptide must adopt a structure with complementary properties with respect to the pocket. Thus, whether a lipoprotein is captured or avoided by LolCDE is likely reflected upon the combinatory effect of the sequence and folding of the N-terminal peptide as well as the shape and surface property of the peptide-accommodating pocket in the transporter. This likely contributes to the highly divergent Lol avoidance signals in different bacteria.

The structures of MacB in different functional states were resolved, and demonstrate how ATP binding causes large-scale conformational changes of the periplasmic domain, presumably harnessing mechanotransmission to drive the movement of MacA in the periplasm and expel the drug substrates[26-29]. The observed conformational change of LolCDE upon vanadate trapping is similar to that of MacB between its nucleotide-free and ATP-bound states[26, 29] (Supplementary Videos 1, 2). In both cases, NBD dimerization causes the upward movement of TM2 and subsequent rearrangement of periplasmic domains, which appear to be the common and distinct features of type VII ABC transporters. However, there are several important differences between MacB and LolCDE. First, while all 8 TMs of MacB move inward for its "bellows-like" function, with two TM1s and two TM2s forming a four-helix bundle in the center (Supplementary Fig. 9a, b), the inward movement in LolCDE is limited to 3 TMs, with two TM2s forming a central two-helix bundle (Fig. 4b). Second, while the rotation of MacB periplasmic domain is facilitated by upward TM2 motion against inward TM1 motion, corresponding rotation in LolE is largely facilitated by the formation of the 90° kink at the periplasmic end of TM2 (Fig. 4c). Third, while MacB moves both TM1 and TM2 to close the periplasmic domains through symmetrical translation and rotation (Supplementary Fig. 9c, d), LolCDE predominantly uses the upward TM2 motion to extrude the bound lipoprotein and produce an asymmetrical movement of the two periplasmic domains which may have additional functions in protecting and reorienting the extracted lipoprotein to facilitate its loading onto LolA. In summary,

all these differences highlight the distinct functions of LolCDE and MacB as membrane extractor and mechanotransducer, respectively.

Acknowledgements

We thank L. Huang, X. Wang, and Z. Jiang from Westlake University cryo-EM facility for help in cryo-EM data acquisition for vanadate-trapped LolCDE. The dataset of nucleotide-free LolCDE was collected at cryo-EM core facility at University of Massachusetts Medical School (UMMS). We are grateful to all Liao lab members for their helpful feedback throughout this project and A. Plummer and A. Culbertson for helpful comments on the manuscript. Y.L. was supported by the Zhejiang Provincial Natural Science Foundation of China (LR20C050001).

Author contribution

M.L. conceived the project. M.L. and Y.L. supervised the project. S.S. and R.Z. performed molecular cloning, protein purification, nanodisc reconstitution, mutagenesis and co-purification. S.S., R.Z. and L.W collected the cryo-EM data. K.S. and C.X. helped cryo-EM data acquisition. S.S processed cryo-EM data and built models. All authors contributed to data analysis. S.S., Y.L. and M.L. wrote the manuscript with the input from all authors.

Author information

The authors declare no competing financial interests. Correspondence and requests for materials should be addressed to Y.L. (liyanyan@westlake.edu.cn) or M.L. (maofu_liao@hms.harvard.edu).

Materials and methods

Cloning, expression and purification of LolCDE. The genes encoding LolC, LolE and LolD with flanking restriction sites BamHI and NotI were amplified individually from *E. coli* K12 genomic DNA by PCR. The C-terminus of LolD was extended using the linker sequence GGGAA and a 6x His tag. LolC, LolE and LolD amplicons were individually inserted into pQlinkN vectors (Addgene). The recombinant vectors pQlinkN-LolD-His, pQlink-LolE and pQlink-LolC were individually digested using the restriction enzymes PacI and SwaI, and the digested products were linked using ligation independent cloning as previously described[30]. The final recombinant vector pQLink-LolCD(6xHis)E was transformed into *E. coli* BL21(DE3) cells for over-expression. Transformed *E. coli* was grown in terrific broth supplemented with 100 µg/ml ampicillin at 37 °C until the cells reached an OD_{600} of ~2. LolCDE expression was induced by addition of 0.1 mM Isopropyl β-D-1-thiogalactopyranoside (IPTG) and the cells were grown at 18 °C for 48 hours. Cells were collected by centrifugation and the pellets resuspended in buffer A (25 mM Tris pH 7.4, 250 mM NaCl and 10% glycerol). Resuspended cell pellets were flash frozen in liquid nitrogen and stored at -80 °C until use. Thawed cells were supplemented with 0.5 mg/ml lysozyme, 0.1 mg/ml DNase I, incubated on ice for 30 minutes, supplemented with protease inhibitors and lysed by passing through an LM20 microfluidizer (Microfluidics) once. Lysed cells were subjected to low-speed centrifugation at 12,000 g for 30 minutes to remove unbroken cells and debris followed by ultracentrifugation at 100,000 g for 1 hour to collect membranes. Membrane pellets were resuspended in buffer A, supplemented with protease inhibitors and solubilized in 1% n-Dodecyl-β-D-Maltoside (Anatrace), for 1 hour at 4 °C. Unsolubilized material was removed by ultracentrifugation at 100,000 g for 1 hour. Solubilized membranes were subjected to affinity column chromatography using Ni-IMAC resin (Profinity) and eluted using buffer containing 25 mM Tris pH 7.4, 150 mM NaCl, 0.05% DDM and 250 mM Imidazole. The eluted protein was further purified by size-exclusion chromatography on a Superdex 200 column in a buffer containing 25 mM Tris, pH7.4, 150 mM NaCl, 0.05% DDM and 5% glycerol.

Co-purification of LolCDE and Lpp. Gene encoding *lpp* was amplified from *E. coli* K-12 genomic DNA. The C-terminal lysine residue (K58) was deleted (LppK58del) to inhibit the formation of a covalent linkage with peptidoglycan and prevent cell toxicity. The fragment of *lpp with* C-terminal Flag tag was inserted into pQLink-LolCDE vector. All site-directed mutations were generated following the protocol of NEB Q5 site-directed mutagenesis kit. The final recombinant vector pQLink-LolCD(6xHis)E-Lpp (C-Flag) was transformed into *E. coli* BL21(DE3) cells for co-expression. The LolCDE–Lpp or relevant mutant proteins were expressed and purified using the same methods as described for LolCDE above. His tag purified LolCDE-Lpp fractions were detected by western blot using anti-His and anti-Flag antibodies.

Nanodisc reconstitution. 1-palmitoyl-2-oleoyl-sn-glycero-3-phosphatidylglycerol (POPG) (Avanti Polar Lipids) in chloroform was dried under argon gas and stored in vacuum overnight. The dried lipid film was re-suspended in nanodisc buffer (25 mM Tris pH 7.4, 150 mM NaCl), sonicated in a water bath for 1 hour (until homogeneous) and solubilized in 25 mM sodium cholate. MSP1D1 membrane scaffold protein and purified LolCDE were added to the reconstitution mixture at a final molar ratio of 1:2:130 (LolCDE: MSP1D1: POPG) and incubated at 4 °C for 1 hour. Detergent was removed by incubation with 0.6 g/ml Bio-Beads SM-2 (Bio-Rad) at 4 °C for 2 hours. Nanodisc-reconstituted LolCDE was further purified by size exclusion chromatography using a Superdex 200 column in nanodisc buffer. The purity of LolCDE in nanodiscs was assessed using SDS-PAGE and negative stain electron microscopy.

ATPase assay. ATPase activity of LolCDE in DDM detergent or nanodiscs was measured using a colorimetric ATPase kit (Sigma Aldrich) according to manufacturer's instructions. Briefly, 1 µg of LolCDE was incubated in 25 mM Tris, pH 8, 150 mM NaCl, 4 mM ATP, and 4 mM $MgCl_2$ for 30 minutes at 37 °C. The reaction was stopped by the addition of 200 µl of reagent provided in the kit, incubated at room temperature for 30 minutes and the absorbance at 620 nm was measured using a SpectraMax M5 spectrophotometer (Molecular Devices).

Phosphate standard curve was constructed using stock solutions provided in the kit according to manufacturer's instructions and used to determine the total concentration of released phosphate. ATPase activities of all samples were determined using the mean value of the samples according to the linear regression of standards. Data was plotted and analyzed in GraphPad Prism 8.

Electron microscopy sample preparation and data acquisition. Nanodisc-embedded LolCDE at a concentration of 1.6 - 2 mg/mL was used for freezing cryo-EM grids. A 2.5 µL volume of sample was applied to glow-discharged Quantifoil R1.2/1.3 holey carbon grids and blotted for 3.5 s at 100% humidity using a Mark IV Vitrobot (Thermo Fisher Scientific) before being plunge frozen in liquid ethane cooled by liquid nitrogen. For vanadate trapping, the samples were incubated in a buffer containing 2 mM ATP, 2 mM $MgCl_2$ and 1 mM sodium orthovanadate for 30 min at room temperature before applying the samples to cryo-EM grids. Cryo-EM images were collected at liquid nitrogen temperature on a Titan Krios (Thermo Fisher Scientific) equipped with a K3 detector (Gatan) and a BioQuantum imaging filter, using image shift and beam tilt to collect one shot per hole and nine holes per stage move. Movies were recorded in super-resolution mode with SerialEM[31] or AutoEMation[32]. A slit width of 20 eV for energy filter was set during the data collection. The details of EM data collection parameters are listed in Supplementary Table 1.

Electron microscopy image processing. EM data were processed as previously described with minor modifications[33]. For both negative-stain EM and cryo-EM, particle images were initially selected using a semi-automated procedure implemented in Simplified Application Managing Utilities for EM Labs (SAMUEL v21.01)[34], and two-dimensional (2D) classification of selected particle images was performed with "samclasscas.py", "samtree2dv3.py" or 2D classification in RELION-3.0[35]. For processing cryo-EM images, dose-fractionated super-resolution movies were binned over 2 × 2 pixels, and beam-induced motion was corrected using the program MotionCor2[36]. Defocus values were calculated using the program CTFFIND4[37]. Initial models for 3D classification were generated by refinement of 2D class averages against a random density using projection matching. 3D classification and refinement were carried out in RELION-3.0. Following two rounds of global 3D classification, masks were constructed to focus 3D classification on LolCDE, omitting the signal from nanodisc. The orientation parameters of the homogenous set of particle images in selected 3D classes were iteratively refined to yield higher resolution maps using the "auto-refine" procedure in RELION. All refinements followed the gold-standard procedure, in which two half datasets are refined independently. The overall resolutions were estimated based on the gold-standard Fourier shell correlation (FSC) = 0.143 criterion. Local resolution variations were estimated from the two half data maps using ResMap[38]. The final map of nucleotide-free LolCDE was subjected to a density-modification procedure[39]. The final map of vanadate-trapped LolCDE was corrected for amplitude information by using "relion_postprocess" in RELION3.0. The detailed workflows of processing the cryo-EM datasets are illustrated in Supplementary Figs. 2c and 6c. The number of particles in each dataset and other details related to data processing are summarized in Supplementary Table 1.

Model Building and refinement. The crystal structure of MacB with ATPγS bound (PDB: 5LIL) was used as a template to generate homology models for LolC and LolE using SWISS-MODEL[40]. The homology models were fit into the cryo-EM maps for LolCDE in the nucleotide-free and nucleotide-bound conformations using UCSF Chimera[41]. Manual adjustment of the models was performed in COOT[42], followed by iterative rounds of real space refinement in PHENIX[43] and manual adjustment in COOT.

The crystal structure of the periplasmic domain of LolC (PDB: 6F3Z) was docked into the corresponding density in our maps, manually adjusted in COOT and real space refined in PHENIX. The refined model for the periplasmic domain of LolC was used as a template to generate a homology model for the periplasmic domain of LolE using SWISS-MODEL. Similarly, a template-independent homology model was generated for LolD. The homology models were fit into their corresponding densities in UCSF Chimera, manually adjusted in COOT and real space refined in PHENIX.

A SMILES string for the triacyl-peptide ligand was generated using the PubChem draw structure tool and restraints for the molecule were generated using PHENIX eLBOW[44]. For the ADP-Vanadate complex, the pdb three-letter-code (AOV) was used to generate restraints in eLBOW. The ligands were roughly fit into their corresponding densities in UCSF Chimera, manually adjusted with the CIF restraints in COOT and real space refined in PHENIX.

Map visualization and structure analysis. Maps were visualized in UCSF Chimera[41] . The nucleotide-free and nucleotide-bound conformations of LolCDE were aligned based on the transmembrane domain using the Matchmaker tool in Chimera. Distances between Cα atoms to measure conformational change induced displacement was measured using the Structure analysis (distances) tool in Chimera. To measure the angle of rotation for the periplasmic domains of LolC a two-dimensional plane was generated using the residues Leu256 and Met175 (Hook) in the nucleotide-free and nucleotide-bound conformations, using the Structure analysis (axes/planes/centroids) tool. The angle between the selected planes was measured using the *angle* command. A similar procedure was used to measure rotation of the periplasmic domain of LolE using the amino acid residues Tyr260 and Leu110. Hydrophobicity of surfaces was measured using the *rangecolor* command. All figures and videos were generated using Chimera.

Data availability

Data supporting the findings of this manuscript are available from the corresponding author upon reasonable request. A reporting summary for this Article is available as a Supplementary Information file. The three-dimensional cryo-EM density maps of *E. coli* LolCDE in nanodiscs have been deposited in the Electron Microscopy Data Bank under accession numbers: EMD-23783 (nucleotide-free) and EMD-23784 (vanadate-trapped). Atomic coordinates for the atomic models of LolCDE have been deposited in the Protein Data Bank under accession numbers: 7MDX (nucleotide-free) and 7MDY (vanadate-trapped).

References

1. Sutcliffe, I.C., Harrington, D.J. & Hutchings, M.I. A phylum level analysis reveals lipoprotein biosynthesis to be a fundamental property of bacteria. *Protein Cell* **3**, 163-170 (2012).
2. Kovacs-Simon, A., Titball, R.W. & Michell, S.L. Lipoproteins of bacterial pathogens. *Infect Immun* **79**, 548-561 (2011).
3. Konovalova, A., Kahne, D.E. & Silhavy, T.J. Outer Membrane Biogenesis. *Annu Rev Microbiol* **71**, 539-556 (2017).
4. Narita, S.I. & Tokuda, H. Bacterial lipoproteins; biogenesis, sorting and quality control. *Biochim Biophys Acta Mol Cell Biol Lipids* **1862**, 1414-1423 (2017).
5. Hooda, Y. & Moraes, T.F. Translocation of lipoproteins to the surface of gram negative bacteria. *Curr Opin Struct Biol* **51**, 73-79 (2018).
6. Nakayama, H., Kurokawa, K. & Lee, B.L. Lipoproteins in bacteria: structures and biosynthetic pathways. *FEBS J* **279**, 4247-4268 (2012).
7. Kurokawa, K. *et al.* Novel bacterial lipoprotein structures conserved in low-GC content gram-positive bacteria are recognized by Toll-like receptor 2. *The Journal of biological chemistry* **287**, 13170-13181 (2012).
8. Hooda, Y., Lai, C.C.L. & Moraes, T.F. Identification of a Large Family of Slam-Dependent Surface Lipoproteins in Gram-Negative Bacteria. *Front Cell Infect Microbiol* **7**, 207 (2017).
9. Okuda, S. & Tokuda, H. Lipoprotein sorting in bacteria. *Annu Rev Microbiol* **65**, 239-259 (2011).
10. Grabowicz, M. & Silhavy, T.J. Redefining the essential trafficking pathway for outer membrane lipoproteins. *Proceedings of the National Academy of Sciences of the United States of America* **114**, 4769-4774 (2017).
11. Nickerson, N.N. *et al.* A Novel Inhibitor of the LolCDE ABC Transporter Essential for Lipoprotein Trafficking in Gram-Negative Bacteria. *Antimicrob Agents Chemother* **62** (2018).
12. Nayar, A.S. *et al.* Novel antibacterial targets and compounds revealed by a high-throughput cell wall reporter assay. *J Bacteriol* **197**, 1726-1734 (2015).
13. McLeod, S.M. *et al.* Small-molecule inhibitors of gram-negative lipoprotein trafficking discovered by phenotypic screening. *J Bacteriol* **197**, 1075-1082 (2015).
14. Narita, S. & Tokuda, H. Overexpression of LolCDE allows deletion of the Escherichia coli gene encoding apolipoprotein N-acyltransferase. *J Bacteriol* **193**, 4832-4840 (2011).
15. Lewenza, S., Mhlanga, M.M. & Pugsley, A.P. Novel inner membrane retention signals in Pseudomonas aeruginosa lipoproteins. *J Bacteriol* **190**, 6119-6125 (2008).
16. Remans, K., Vercammen, K., Bodilis, J. & Cornelis, P. Genome-wide analysis and literature-based survey of lipoproteins in Pseudomonas aeruginosa. *Microbiology (Reading)* **156**, 2597-2607 (2010).
17. Schulze, R.J. & Zuckert, W.R. Borrelia burgdorferi lipoproteins are secreted to the outer surface by default. *Mol Microbiol* **59**, 1473-1484 (2006).
18. Hooda, Y., Shin, H.E., Bateman, T.J. & Moraes, T.F. Neisserial surface lipoproteins: structure, function and biogenesis. *Pathog Dis* **75** (2017).
19. Greene, N.P., Kaplan, E., Crow, A. & Koronakis, V. Antibiotic Resistance Mediated by the MacB ABC Transporter Family: A Structural and Functional Perspective. *Front Microbiol* **9**, 950 (2018).
20. Thomas, C. *et al.* Structural and functional diversity calls for a new classification of ABC transporters. *FEBS letters* (2020).
21. Thomas, C. & Tampe, R. Structural and Mechanistic Principles of ABC Transporters. *Annual review of biochemistry* **89**, 605-636 (2020).
22. Kaplan, E., Greene, N.P., Crow, A. & Koronakis, V. Insights into bacterial lipoprotein trafficking from a structure of LolA bound to the LolC periplasmic domain. *Proceedings of the National Academy of Sciences of the United States of America* **115**, E7389-E7397 (2018).
23. Armbruster, K.M. & Meredith, T.C. Identification of the Lyso-Form N-Acyl Intramolecular Transferase in Low-GC Firmicutes. *J Bacteriol* **199** (2017).

24. Braun, V. & Rehn, K. Chemical characterization, spatial distribution and function of a lipoprotein (murein-lipoprotein) of the E. coli cell wall. The specific effect of trypsin on the membrane structure. *Eur J Biochem* **10**, 426-438 (1969).
25. Li, G.W., Burkhardt, D., Gross, C. & Weissman, J.S. Quantifying absolute protein synthesis rates reveals principles underlying allocation of cellular resources. *Cell* **157**, 624-635 (2014).
26. Crow, A., Greene, N.P., Kaplan, E. & Koronakis, V. Structure and mechanotransmission mechanism of the MacB ABC transporter superfamily. *Proceedings of the National Academy of Sciences of the United States of America* **114**, 12572-12577 (2017).
27. Okada, U. *et al.* Crystal structure of tripartite-type ABC transporter MacB from Acinetobacter baumannii. *Nat Commun* **8**, 1336 (2017).
28. Yang, H.B. *et al.* Structure of a MacAB-like efflux pump from Streptococcus pneumoniae. *Nat Commun* **9**, 196 (2018).
29. Fitzpatrick, A.W.P. *et al.* Structure of the MacAB-TolC ABC-type tripartite multidrug efflux pump. *Nat Microbiol* **2**, 17070 (2017).
30. Scheich, C., Kummel, D., Soumailakakis, D., Heinemann, U. & Bussow, K. Vectors for co-expression of an unrestricted number of proteins. *Nucleic Acids Res* **35**, e43 (2007).
31. Schorb, M., Haberbosch, I., Hagen, W.J.H., Schwab, Y. & Mastronarde, D.N. Software tools for automated transmission electron microscopy. *Nat Methods* **16**, 471-477 (2019).
32. Lei, J. & Frank, J. Automated acquisition of cryo-electron micrographs for single particle reconstruction on an FEI Tecnai electron microscope. *J Struct Biol* **150**, 69-80 (2005).
33. Mi, W. *et al.* Structural basis of MsbA-mediated lipopolysaccharide transport. *Nature* **549**, 233-237 (2017).
34. Ru, H. *et al.* Molecular Mechanism of V(D)J Recombination from Synaptic RAG1-RAG2 Complex Structures. *Cell* **163**, 1138-1152 (2015).
35. Scheres, S.H. RELION: implementation of a Bayesian approach to cryo-EM structure determination. *J Struct Biol* **180**, 519-530 (2012).
36. Zheng, S.Q. *et al.* MotionCor2: anisotropic correction of beam-induced motion for improved cryo-electron microscopy. *Nat Methods* **14**, 331-332 (2017).
37. Rohou, A. & Grigorieff, N. CTFFIND4: Fast and accurate defocus estimation from electron micrographs. *J Struct Biol* **192**, 216-221 (2015).
38. Kucukelbir, A., Sigworth, F.J. & Tagare, H.D. Quantifying the local resolution of cryo-EM density maps. *Nat Methods* **11**, 63-65 (2014).
39. Terwilliger, T.C., Ludtke, S.J., Read, R.J., Adams, P.D. & Afonine, P.V. Improvement of cryo-EM maps by density modification. *Nat Methods* **17**, 923-927 (2020).
40. Bertoni, M., Kiefer, F., Biasini, M., Bordoli, L. & Schwede, T. Modeling protein quaternary structure of homo- and hetero-oligomers beyond binary interactions by homology. *Sci Rep* **7**, 10480 (2017).
41. Pettersen, E.F. *et al.* UCSF Chimera--a visualization system for exploratory research and analysis. *J Comput Chem* **25**, 1605-1612 (2004).
42. Emsley, P., Lohkamp, B., Scott, W.G. & Cowtan, K. Features and development of Coot. *Acta Crystallogr D Biol Crystallogr* **66**, 486-501 (2010).
43. Adams, P.D. *et al.* PHENIX: a comprehensive Python-based system for macromolecular structure solution. *Acta Crystallogr D Biol Crystallogr* **66**, 213-221 (2010).
44. Moriarty, N.W., Grosse-Kunstleve, R.W. & Adams, P.D. electronic Ligand Builder and Optimization Workbench (eLBOW): a tool for ligand coordinate and restraint generation. *Acta Crystallogr D Biol Crystallogr* **65**, 1074-1080 (2009).

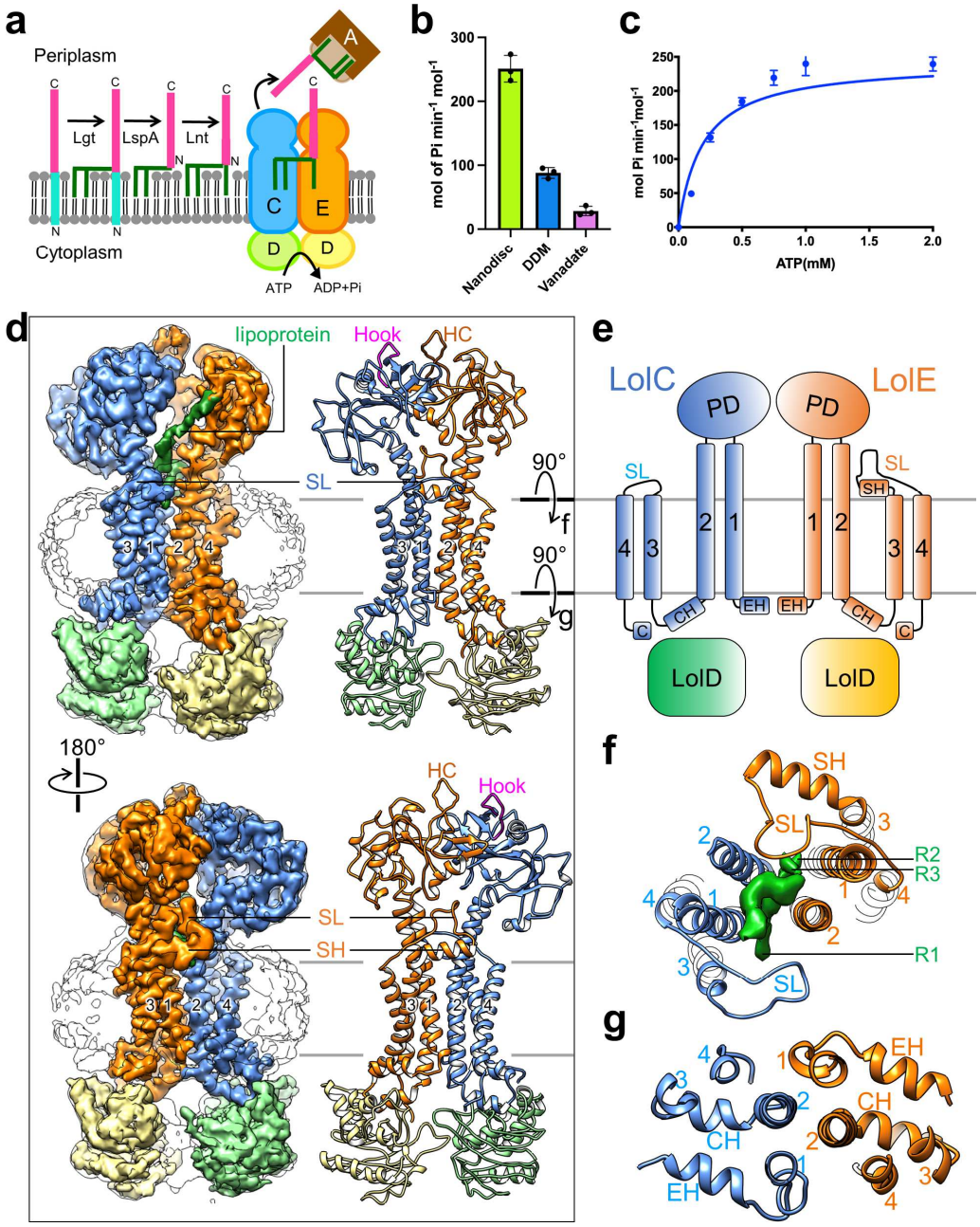

Fig. 1 Biochemical and cryo-EM studies of LolCDE. a Diagram of the steps of lipoprotein biogenesis in the inner membrane, including three enzymatic processing steps, LolCDE-mediated extraction, and delivery to LolA. The Lol proteins are labeled with letters. **b** ATPase activity of LolCDE in nanodiscs, in DDM, and in nanodiscs with 0.1 mM vanadate. Each point represents mean ± s.d. of three separate measurements. **c** ATPase activities of LolCDE in nanodiscs. Each point represents mean ± s.d. of three separate measurements. **d** Cryo-EM map filtered at 3.8-Å resolution and model of LolCDE, viewed from the front (top) and back (bottom). LolC, LolE, two LolD subunits, and lipoprotein are colored separately. Nanodisc is shown as outline. The boundaries of the inner membrane are indicated by gray lines. Hook in LolC, Hook counterpart (HC) in LolE, shoulder loop (SL) and shoulder helix (SH) are indicated. Transmembrane helices are labeled with numbers. **e** Topology of LolCDE. **f, g** Views perpendicular to the membrane plane of the cross sections indicated in (**d**).

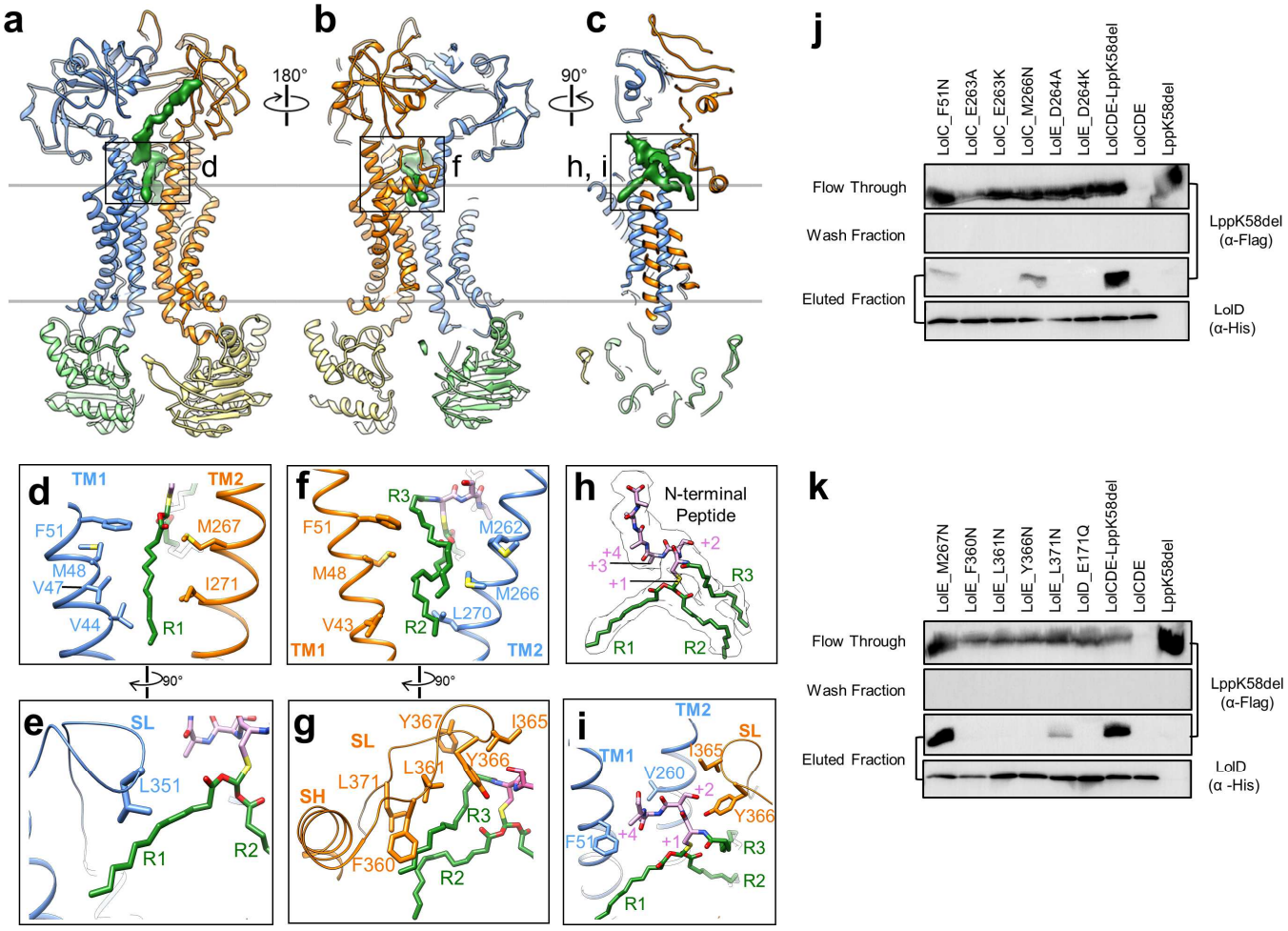

Fig. 2 Lipoprotein interaction with LolCDE. a, b, c Model of LolCDE with the cryo-EM density of lipoprotein (green), shown as front (**a**), back (**b**) and sectional side (**c**) views. Lol proteins are colored as in Fig. 1. **d-i** Close-up views of the selected areas indicated in (**a-c**). The lipoprotein is shown with the N-terminal peptide in purple and three acyl chains in green: the N-terminal R3 and cysteine side chain-connected R1 and R2. SH, shoulder helix (only in LolE); SL, shoulder loop (in LolC and LolE). **j, k** Co-purification assay to test Lpp binding to wild-type and mutant LolCDE. LppK58del without the C-terminal lysine residue was used to prevent cell toxicity. Except the last two lanes, where only wild-type LolCDE or LppK58del was individually expressed, all lanes show the results from co-expression of LolCDE and LppK58del. LolCDE was purified using Ni-NTA via the His tag on LolD. Flow-through, wash and elute were analyzed by western blot. Data are representative of 3 independent experiments.

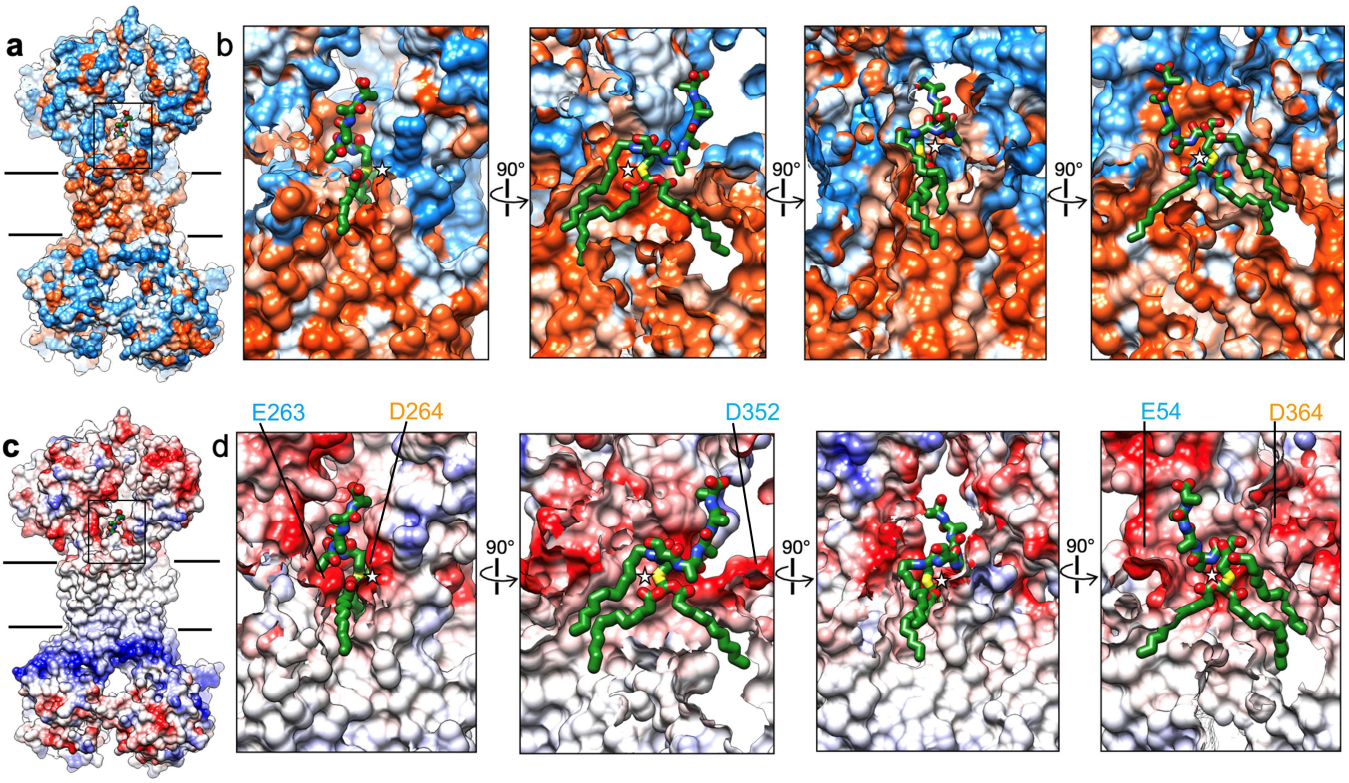

Fig. 3 Hydrophobic and electrostatic surface properties of lipoprotein binding site. a Hydrophobic surface representation of LolCDE, showing hydrophobic (orange) and hydrophilic (blue) areas. **b** Close-up sectional views from 4 orthogonal angles of the area indicated in (**a**). **c** Electrostatic surface representation of LolCDE, showing areas of positive (blue) and negative (red) charge. **d** Close-up sectional views from 4 orthogonal angles of the area indicated in (**c**). Lipoprotein is shown as green stick. The cysteine residue at +1 position is marked with a star. Negatively charged residues near the lipoprotein are indicated.

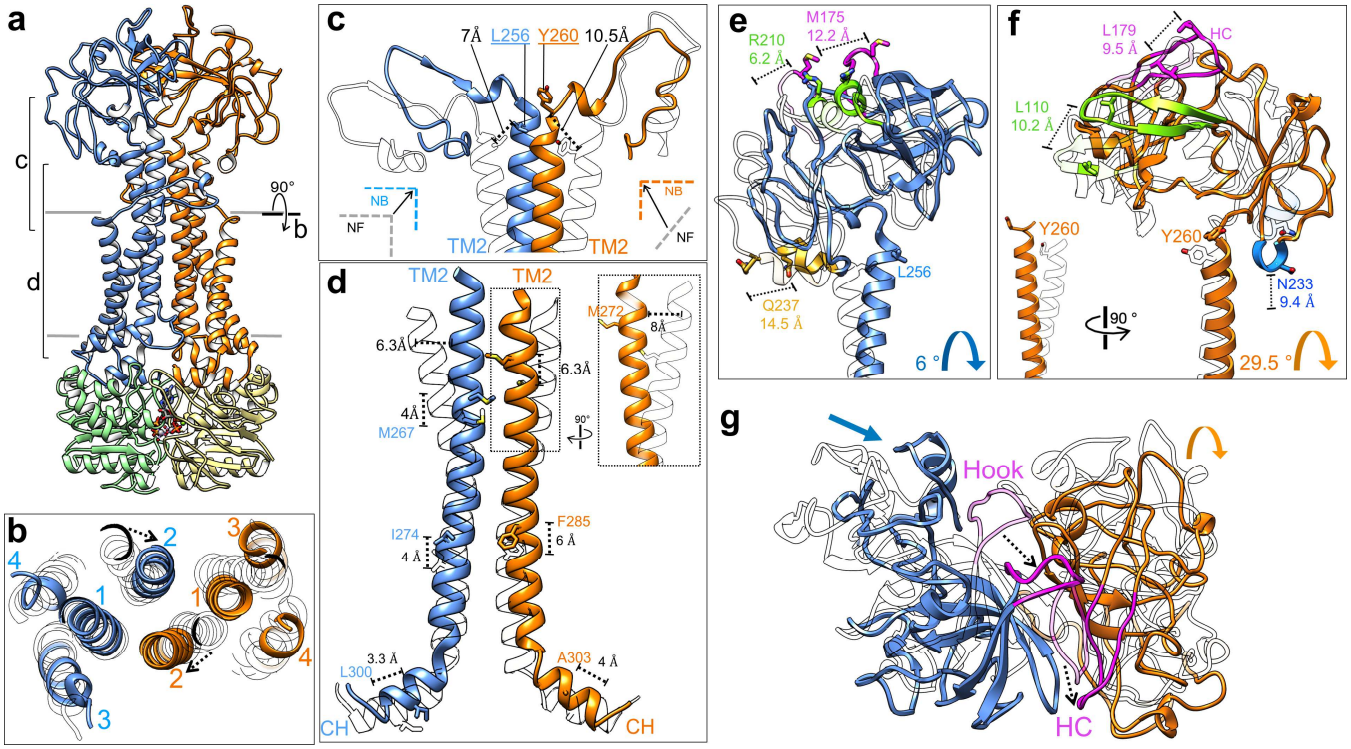

Fig. 4 Conformational changes in LolCDE upon vanadate trapping. a Cryo-EM structure of vanadate-trapped LolCDE with subunits colored as in Fig. 1. **b** Cross-sectional view perpendicular to the membrane plane indicated in (**a**). **c** T-shaped structure formed by the 90° kinks of both TM2 helices. Displacement of the Cα atoms of selected residues is shown. **d** Propagation of upward movement from coupling helix (CH) to TM2, measured as displacement of Cα atoms of indicated residues. Towards the N-terminal region, both TM2 helices undergo inward movement. The more pronounced inward shift of the TM2 in LolE is highlighted in dotted boxes. **e** Translation and rotation of the periplasmic domain of LolC is illustrated by comparison of nucleotide-free (gray) and vanadate-trapped (color) LolCDE. Selected structural regions are highlighted and the displacement of Cα atoms of indicated residues shown. **f** Same as (**e**), except for the periplasmic domain of LolE. **g** Top-down view of periplasmic domains showing overall conformational changes. Hook in LolC and the hook counterpart (HC) in LolE are colored magenta.

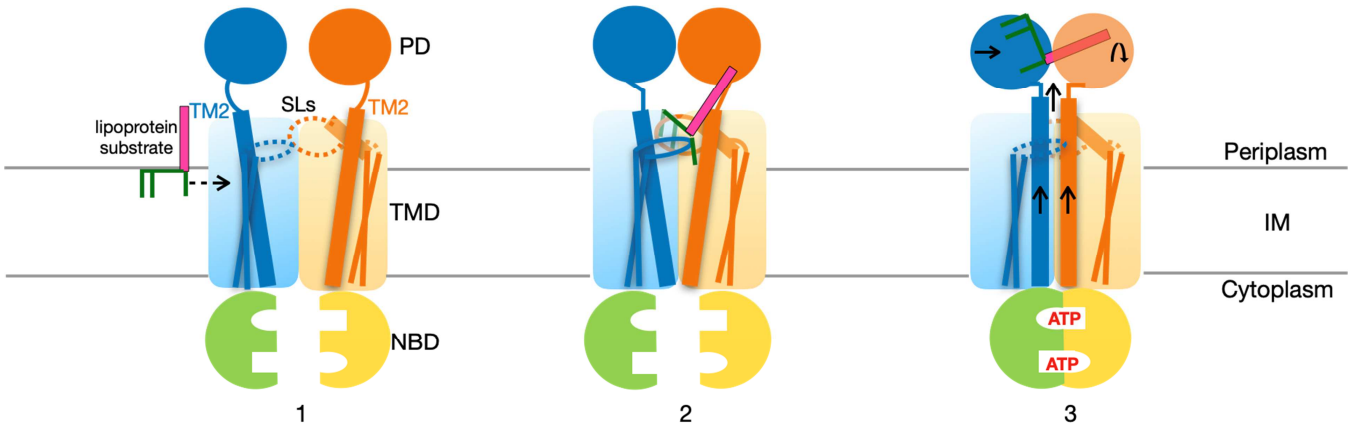

Fig. 5 Proposed model for LolCDE-driven lipoprotein extraction from the inner membrane of *E. coli*. Lol proteins and lipoproteins are colored as in Fig. 1. See text for description of proposed steps for lipoprotein transport. SL, shoulder loop (dotted oval); PD, periplasmic domain; TMD, transmembrane domain; NBD, nucleotide-binding domain; IM, inner membrane.

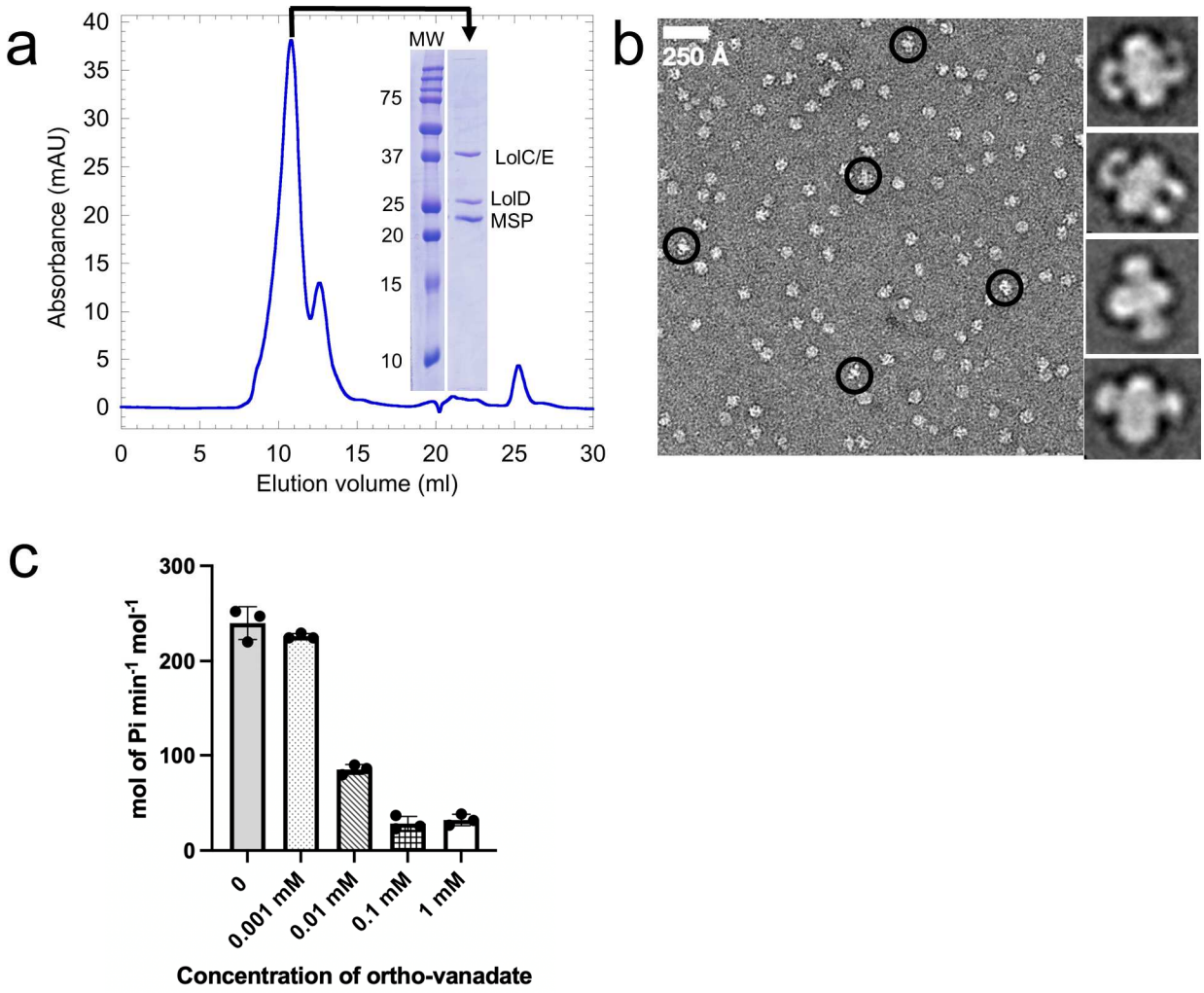

Supplementary Figure 1. Purification and functional characterization of LolCDE in nanodiscs. a, Size exclusion chromatography profile of LolCDE in lipid nanodiscs and SDS-PAGE of the peak fraction shown in inset. **b**, Representative negative-stain EM image and 2D class averages of LolCDE in nanodiscs. **c**, Inhibition of ATPase activity of nanodisc-embedded LolCDE with increasing concentration of sodium orthovanadate.

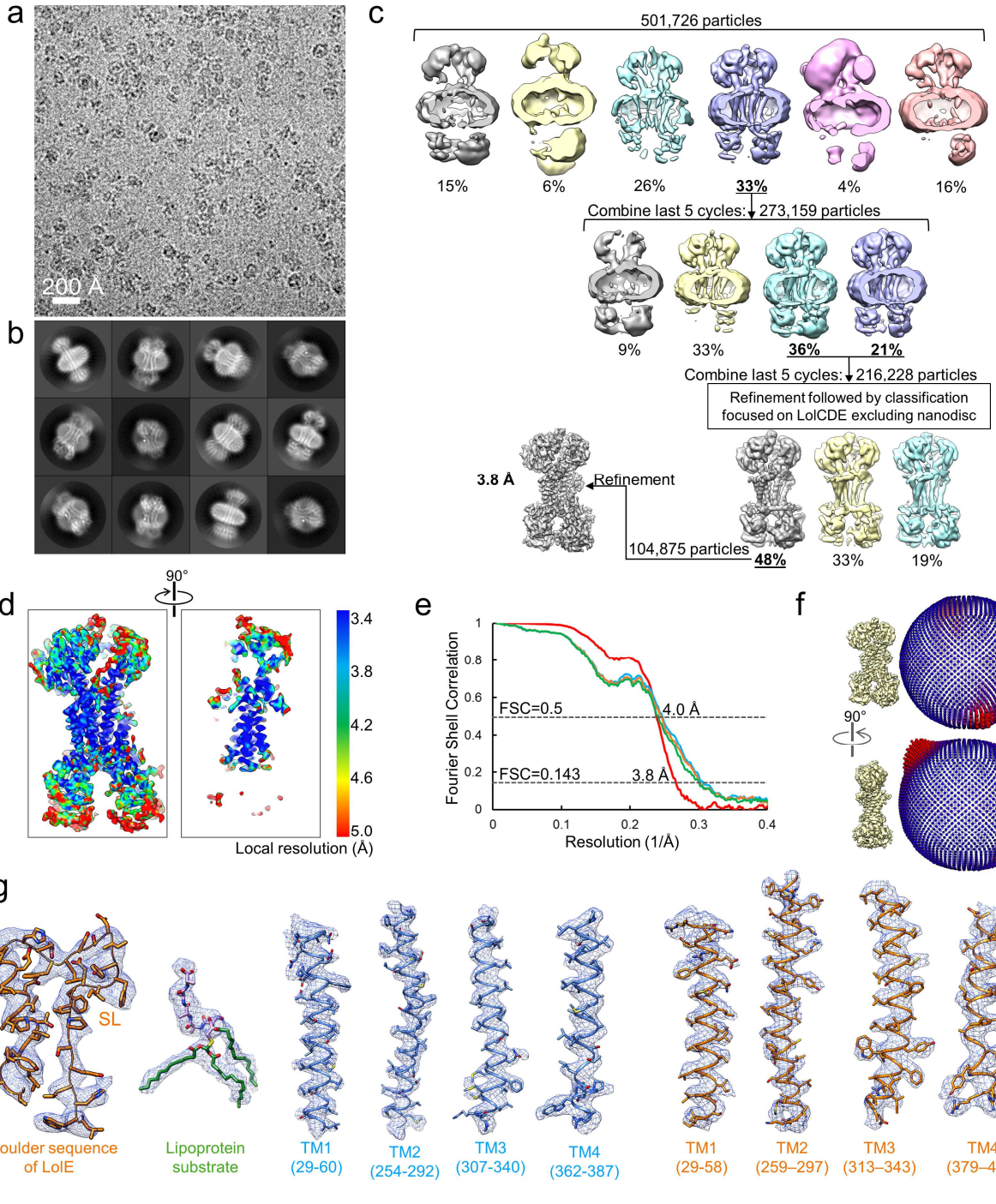

Supplementary Figure 2. Single-particle cryo-EM study of nucleotide-free LolCDE in nanodiscs. a, Representative cryo-EM image of LolCDE in nanodiscs. **b**, Two-dimensional class averages of cryo-EM particle images. **c**, Three-dimensional classification and refinement of cryo-EM particle images. **d**, Local resolution of the final cryo-EM map. **e**, Fourier shell correlation (FSC) curves: gold-standard FSC curve between the two half maps with indicated resolution at FSC = 0.143 (red); FSC curve between the model and the final map with indicated resolution at FSC = 0.5 (blue); FSC curve between half map 1 (orange) or half map 2 (green) and the model refined against half map 1. **f**, Angular distribution of particle images included in the final 3D reconstruction. **g**, Superimposition of cryo-EM densities and the model for selected regions.

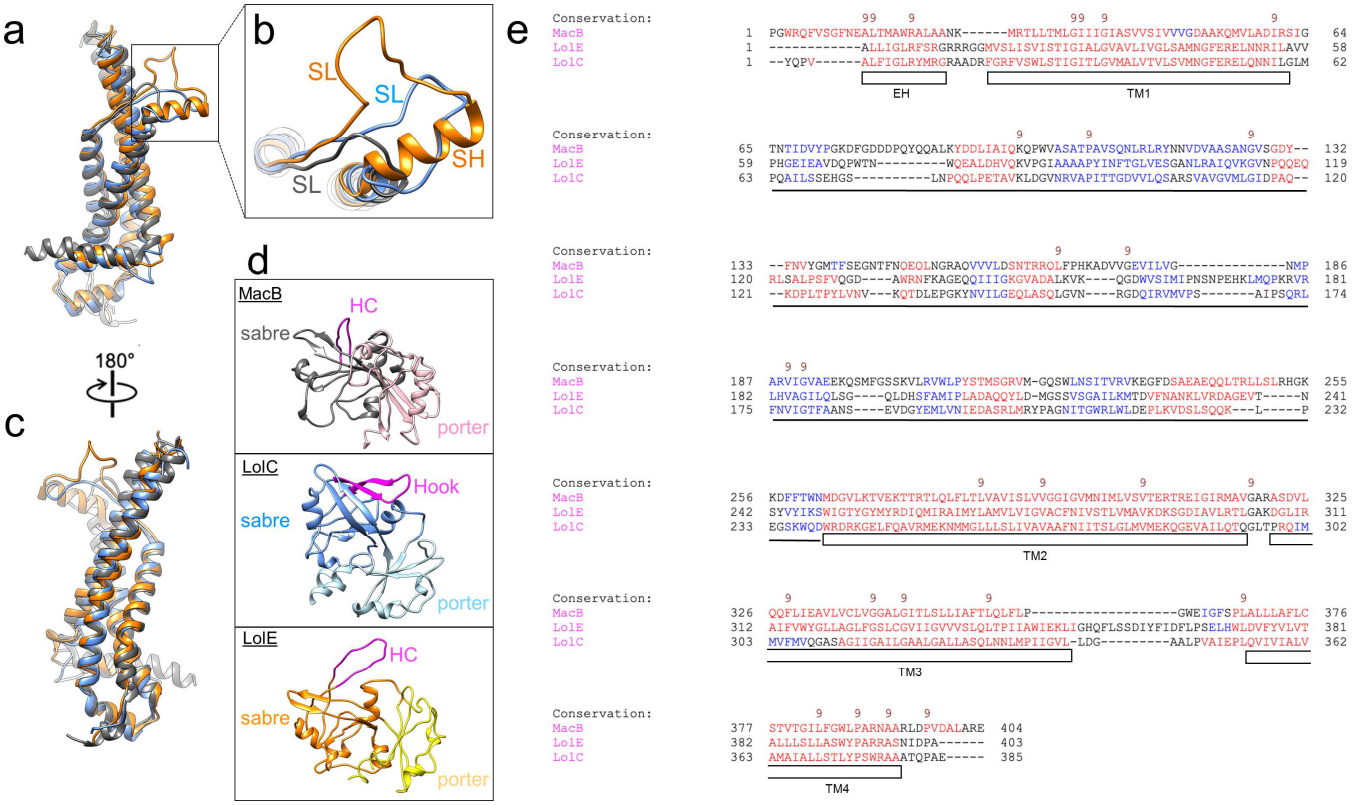

Supplementary Figure 3. Comparison of LolC, LolE and MacB. a, Superimposition of the TMDs of LolC (blue), LolE (orange) and MacB (grey, PDB: 5LIL). **b**, Close-up view of the shoulder loop (SH) region. **c**, 180° rotated view of (**a**). **d**, Structures of the periplasmic domains of MacB, LolC and LolE, oriented based on TMD alignment in (**a**). The porter and sabre subdomains, as well as Hook (in LolC) and Hook counterparts (HC, in MacB and LolE) are highlighted. **e**, Sequence alignment of LolC, LolE and MacB from *E. coli*, conducted using PROMALS3D. Predicated secondary structure elements are colored in red (α-helix) and blue (β-strand). The first line in each block shows conservation indices for positions with a conservation index above 4 (9 being highly conserved).

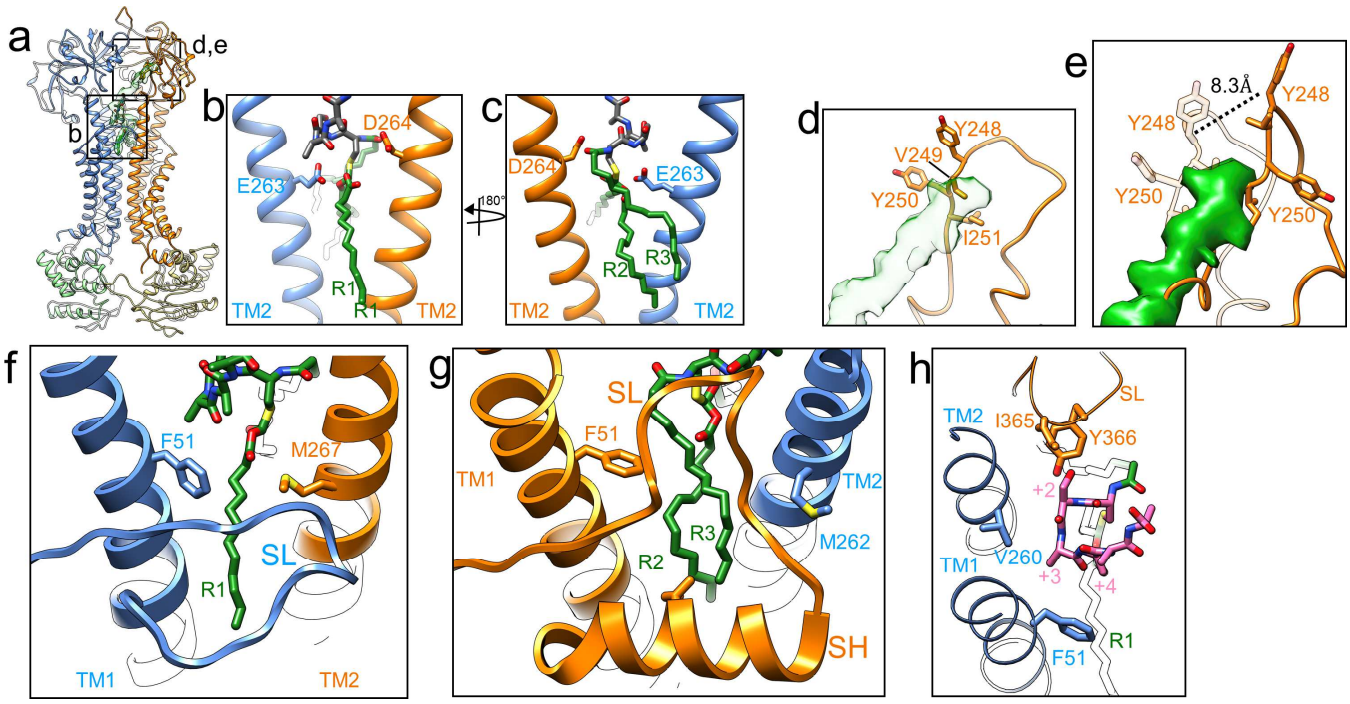

Supplementary Figure 4. Structural details of LolCDE. a, Structure of nucleotide-free LolCDE in nanodiscs. **b**, **c**, Close-up views of lipoprotein binding pockets as indicated in (**a**), showing two negatively charged residues near +1 cysteine. **d**, Close-up view of the lipoprotein linker interacting loop in the periplasmic domain of LolE, as indicated in (**a**), with the linker in transparent green. **e**, Same region as in (**d**), shown as superimposition of nucleotide-free (transparent) and vanadate-trapped (solid) conformation. The displacement of Tyr248 upon vanadate trapping is indicated. **f**, Lipoprotein binding front pocket enclosing acyl chain R1. The distance between the Cα atoms of LolC-F51 and LolE-M267 is 14.9 Å. **g**, Lipoprotein binding back pocket enclosing acyl chains R2 and R3. The distance between LolE-F51 and LolC-M262 is 17.6 Å. **h**, N-terminal lipoprotein peptide enclosing pocket composed of LolC-TM1, LolC-TM2 and LolE-TM2.

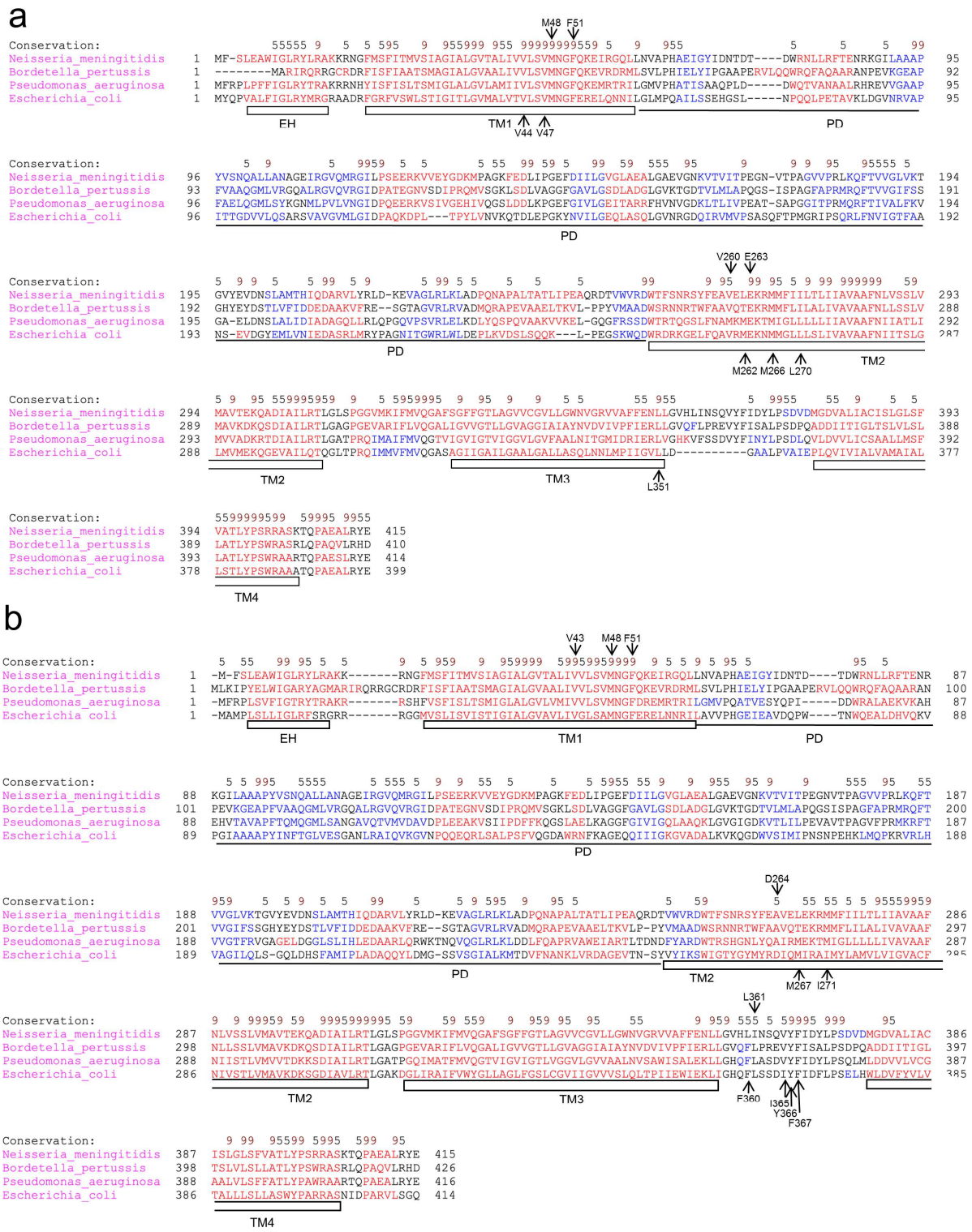

Supplementary Figure 5. Multiple sequence alignment for LolC and LolE. a, Alignment of the amino acid sequences of LolC from four different Gram-negative bacteria. The amino acid residues involved in lipoprotein binding are indicated. The alignment was conducted using PROMALS3D. Predicated secondary structure elements are colored in red (α-helix) and blue (β-strand). **b**, Same as (**a**), except for LolE. The first line in each block shows conservation indices for positions with a conservation index above 4 (9 being highly conserved).

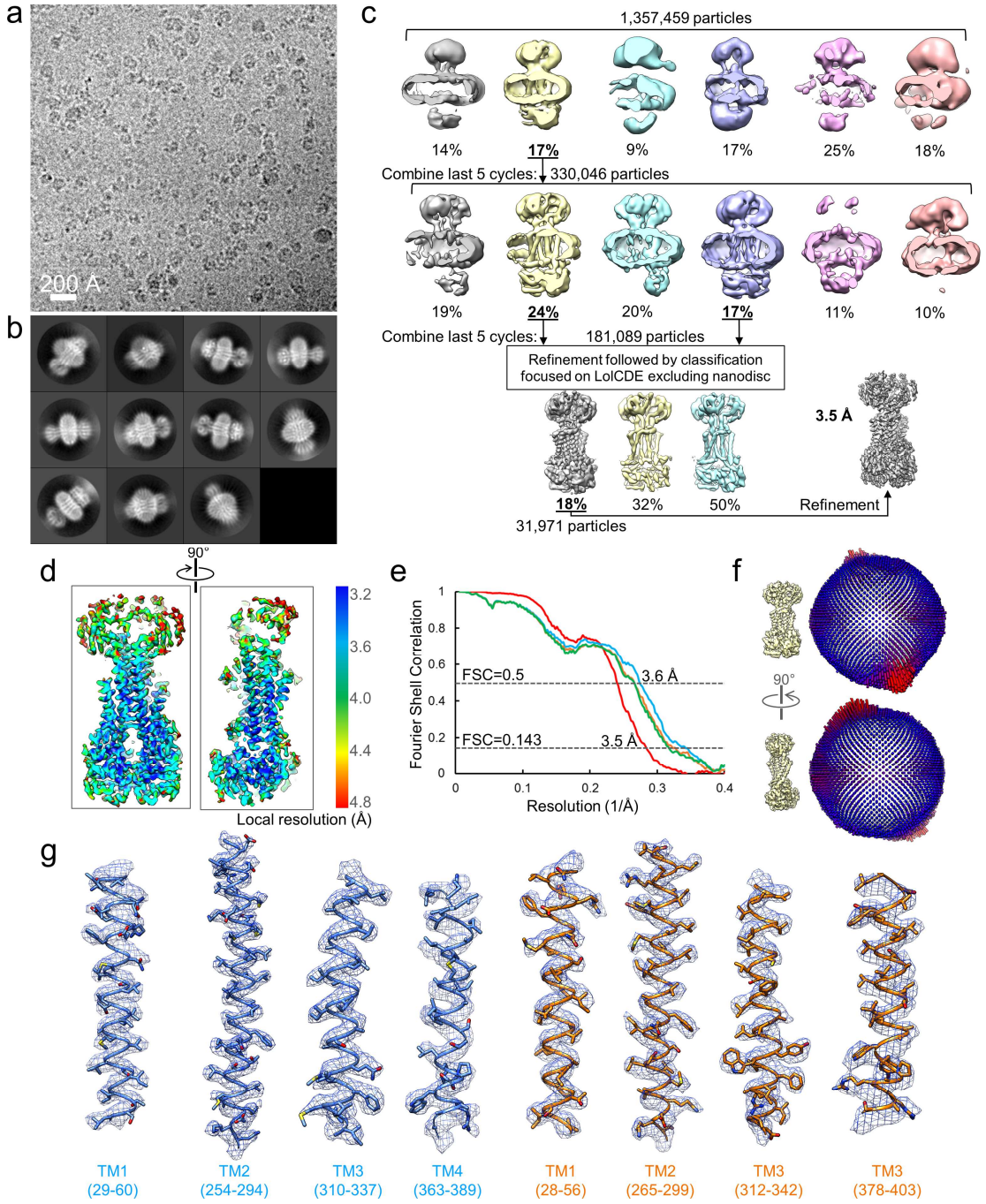

Supplementary Figure 6. Single-particle cryo-EM study of vanadate-trapped LolCDE in nanodiscs. a, Representative cryo-EM image of nanodisc-embedded LolCDE with vanadate trapping. **b**, Two-dimensional class averages of cryo-EM particle images. **c**, Three-dimensional classification and refinement of cryo-EM particle images. **d**, Local resolution of the final cryo-EM map. **e**, Fourier shell correlation (FSC) curves: gold-standard FSC curve between the two half maps with indicated resolution at FSC = 0.143 (red); FSC curve between the model and the final map with indicated resolution at FSC = 0.5 (blue); FSC curve between half map 1 (orange) or half map 2 (green) and the model refined against half map 1. **f**, Angular distribution of particle images included in the final 3D reconstruction. **g**, Superimposition of cryo-EM densities and the model for selected regions.

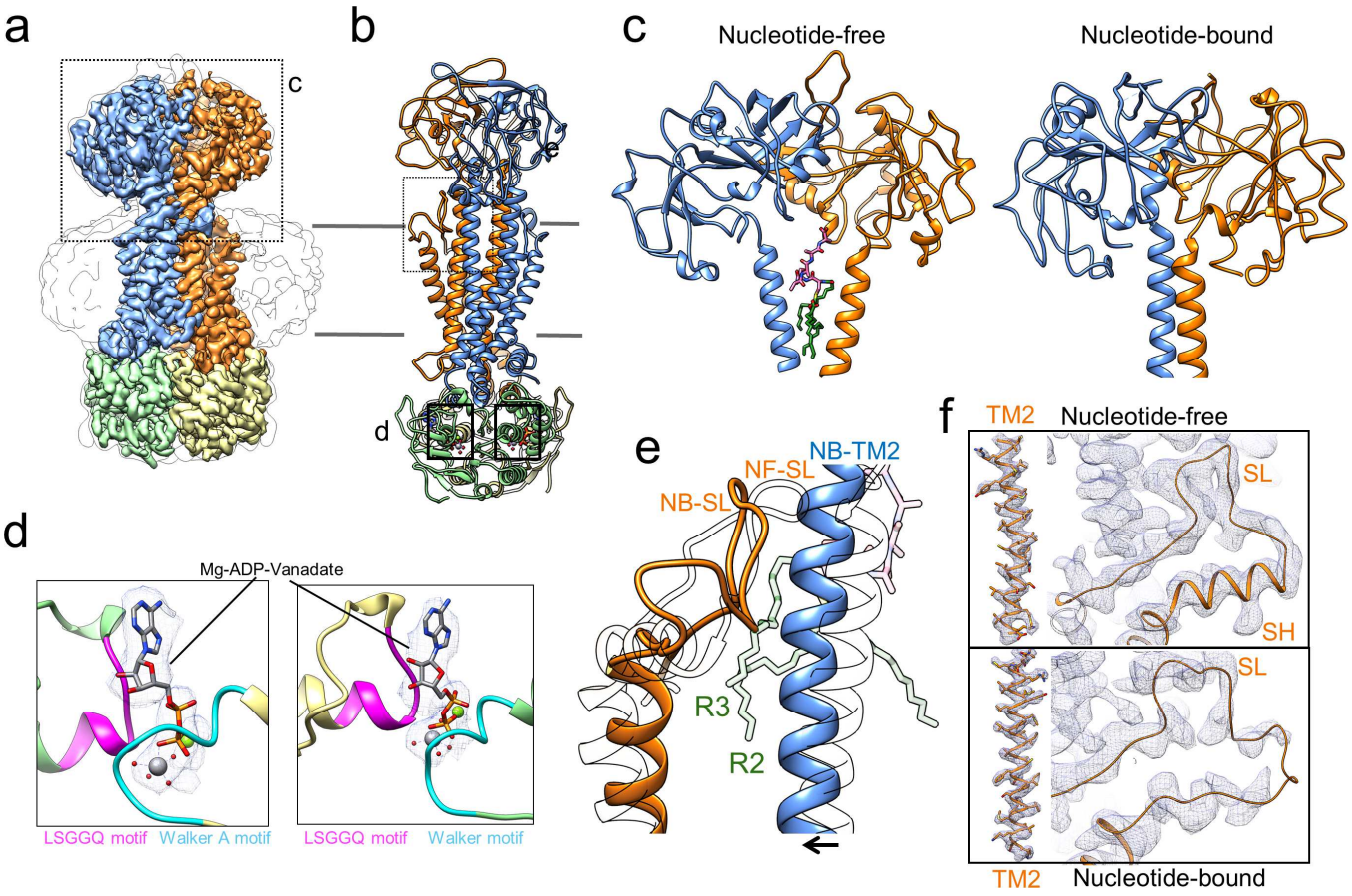

Supplementary Figure 7. Conformational changes of LolCDE induced by vanadate trapping. a, Surface side view of cryo-EM map of vanadate-trapped LolCDE in nanodiscs, filtered at 3.5-Å resolution and colored as in Fig. 1. **b**, 90° rotated side view of model. **c**, Periplasmic region of LolCDE as indicated in (**a**), in nucleotide-free and vanadate-trapped conformations. **d**, Close-up views of the model of two ATP binding sites as indicated in (**b**), shown as superimposition with the EM density of ADP-vanadate complex that is trapped between Walker A and signature motif. **e**, Comparison of the nucleotide-free and vanadate-trapped LolCDE in the region of the shoulder loop (SL) of LolE, as indicated in (**b**), showing blockage of substrate access to SL by the inward movement of the TM2 of LolC. Nucleotide-free conformation is shown as transparent. **f**, Cryo-EM density (gray mesh, contoured at 5.4σ) of the shoulder helix (SH) and SL of LolE in the nucleotide-free (top) and vanadate-trapped (bottom) conformations. The EM densities of the TM2 of LolE in two conformations are contoured at 5.4σ for comparison.

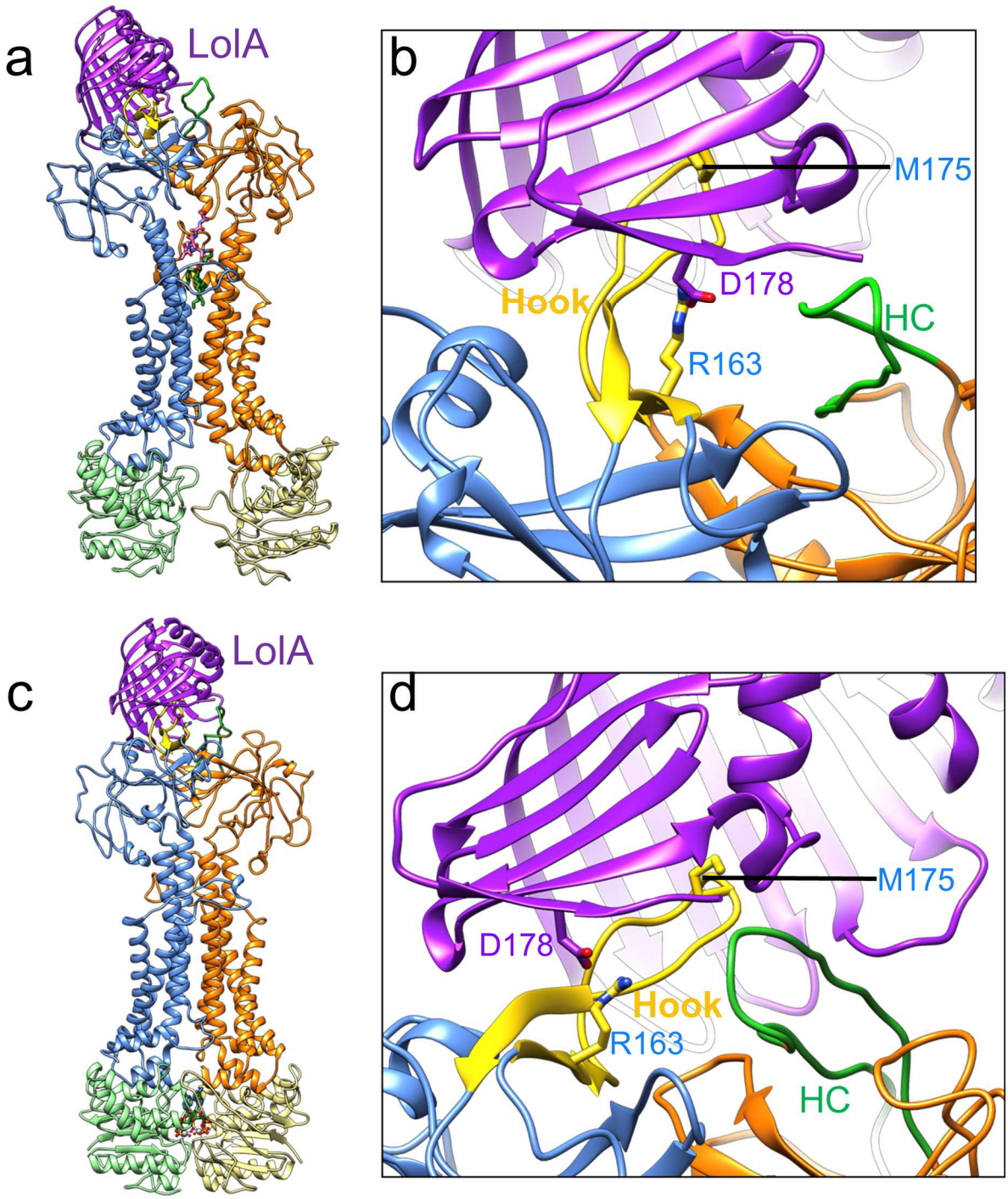

Supplementary Figure 8. Composite models of LolCDE-LolA complex. a, Composite model of LolCDE-LolA in nucleotide-free state, generated by docking LolA on the nucleotide-free conformation of LolCDE. The periplasmic domain of LolC (LolC-PD) from the crystal structure of the LolC-PD-LolA complex (PDB: 6F3Z) was superimposed with LolC-PD in LolCDE. **b**, Close-up view of the binding interface of LolC-LolA with the Hook and pad on LolC highlighted in yellow. The Hook conterpart in LolE is colored green. Key residues implicated in LolA-LolC interaction are indicated. **c, d**, Same as (**a**) and (**b**), except for vanadate-trapped conformation of LolCDE.

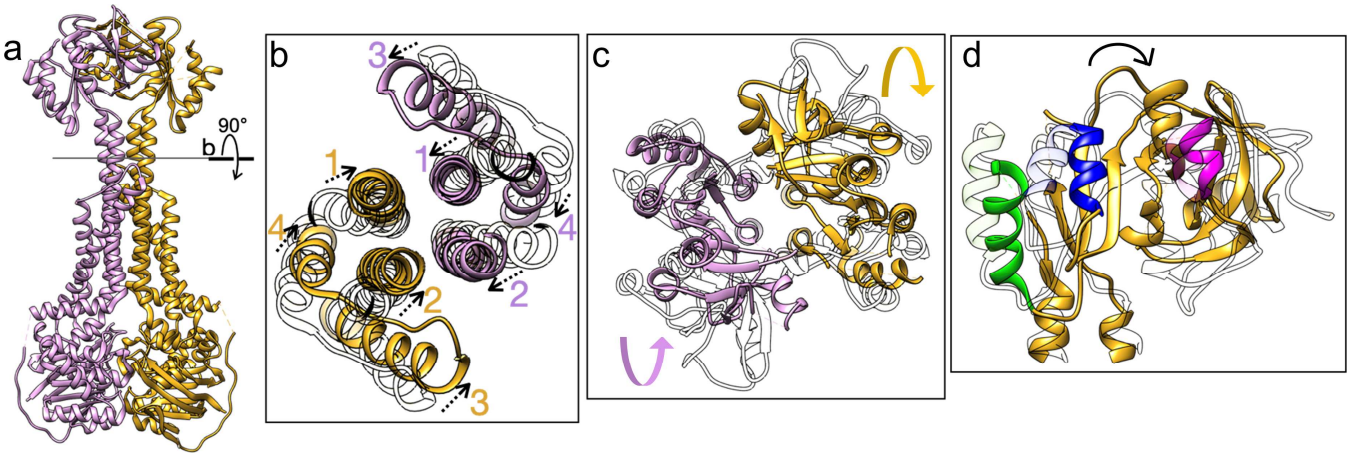

Supplementary Figure 9. Conformational changes of MacB induced by ATP binding. a, MacB in ATP-bound conformation (PDB: 5LJ7). **b**, Sectional view showing TM helices in the nucleotide-free (transparent) and nucleotide-bound (color) conformations. TM2 undergoes an inward and upward conformational shift, while TM1, TM3 and TM4 all shift inward. **c**, Top-down view showing the motion of the periplasmic domains in nucleotide-free (transparent) and nucleotide-bound (color) conformation. The direction of rotation is indicated by arrows. **d**, Side view of one periplasmic domain, highlighting the shifts of various structural elements.

672 **Supplementary Table 1. Cryo-EM structure determination parameters and model statistics.**
673

	Nucleotide-free LolCDE	Vanadate-trapped LolCDE
	PDB ID: 7MDX	PDB ID: 7MDY
	EMDB ID: 23783	EMDB ID: 23784
Data collection and processing		
Microscope	Titan Krios (UMMS)	Titan Krios (Westlake)
Detector	K3 Summit	K3 Summit
Magnification	81,000	81,000
Voltage (kV)	300	300
Electron exposure ($e^-/Å^2$)	46.4	50
Defocus range (μm)	-1 to -2.5	-1 to -2.2
Pixel size (Å)	1.06	1.087
Symmetry imposed	C1	C1
Initial particle images (no.)	501,726	1,357,459
Final particle images (no.)	104,875	31,971
Map resolution (Å)	3.8	3.5
FSC threshold	0.143	0.143
Map resolution range (Å)	3.4 - 5.0	3.2 - 4.8
Refinement		
Initial model used (pdb id)	5LIL, 6F3Z	5LIL, 6F3z
Model resolution (Å) FSC threshold	4.0 0.5	3.6 0.5
Map sharpening B factor (Å)	N/A	-126
Model composition Non-hydrogen atoms Protein residues Ligands Mg	 9507 1236 1 0	 9741 1266 2 2
B-factors (Å) Protein Ligand	 150.4 104.58	 60.96 38.28
R.M.S deviations Bond length (Å) Bond angles (°)	 0.002 0.549	 0.004 0.772
Validation MolProbity score Clashscore Poor rotamers (%)	 2.08 11.19 0.00	 2.37 9.38 2.41
Ramachandran plot Favored (%) Allowed (%) Outliers (%)	 91.01 8.99 0.00	 88.75 11.17 0.08

674
675

Supplementary Video 1. Conformational transition between nucleotide-free and vanadate-trapped *E. coli* LolCDE in nanodiscs. The animation shows a morph between the nucleotide-free and nucleotide-bound states of LolCDE. The subunits are color coded as in the manuscript figures with the LolC-hook shown in magenta. The lipoprotein substrate and ADP-vanadate are omitted.

Supplementary Video 2. Conformational transition between nucleotide-free and ATP-bound MacB. The animation shows a morph between the nucleotide-free (PDB: 5NIL) and ATP-bound (PDB: 5LJ7) conformations of MacB.